Materials Advances

ROYAL SOCIETY OF CHEMISTRY

PAPER

View Article Online
View Journal | View Issue



Cite this: *Mater. Adv.*, 2025, **6**, 7884

# Adipose tissue-derived ECM hydrogels as a 3D platform for neural differentiation and brain diseases

Kyriaki Stampouli,[ab] Lina Papadimitriou,[a] Andrea García-Lizarribar,[c] Iratxe Madarieta,[c] Beatriz Olalde[c] and Anthi Ranella[*a]

The interplay between the extracellular matrix and cells significantly impacts cellular survival, proliferation, and differentiation. Cell growth within 3D scaffolds, particularly hydrogels that mimic cellular microenvironments, offers more relevant insights into tissue development compared to traditional 2D systems. This study explores the behavior of neural stem cells and their differentiation within 3D pure adipose tissue derived-ECM (adECM) hydrogels. These hydrogels provide both physical and biochemical cues that closely resemble the 3D microarchitecture of native tissues. Encapsulating neuroectodermal NE-4C cells in adECM hydrogels at different concentrations revealed intriguing divergent cellular responses. While variations in the fiber structure and pore formation between hydrogels did not significantly affect cell survival, they notably influenced the differentiation process. Analysis of neural-lineage-specific markers, such as tubulinβIII and GFAP, demonstrated divergent differentiation outcomes. This biologically derived, tissue-specific 3D platform enables *in vitro* study of neural differentiation and lays the groundwork for future neural models relevant to regenerative medicine and neurodegenerative research.

Received 2nd April 2025,
Accepted 6th September 2025

DOI: 10.1039/d5ma00310e

rsc.li/materials-advances



## 1. Introduction

Over the past decades, over 92% of therapies from animal trials have failed to translate into human therapy, particularly for neurological diseases,[1] highlighting the need for improved research methods in this area. Combining this with the 3R policy (refine, reduce, and replace the use of animals as experimental models), it is evident that there is a need for more innovative and realistic *in vitro* models.[2] These models should precisely recapitulate the *in vivo* conditions in order to bridge the gap between preclinical research outcomes and human treatments. Neurodegenerative diseases (NDDs), like Alzheimer's disease and related dementia, were ranked the 7th most common cause of death in 2019, according to WHO[3] with a high economic, social, and psychological burden. Although the mechanisms of NDDs have been extensively studied, many pathways remain unclear and research is ongoing to better understand these diseases and discover novel therapies.

Advances in materials science have driven the development of 3-dimensional (3D) models that can mimic the natural cellular microenvironment. Traditional 2D models fail to reproduce the physical, genetic, and biochemical attributes of the native tissue that are needed during the neurodevelopment.[4] The scientific community has developed 3D biomaterial models to enhance the extracellular environment providing precise cellular microenvironment representation and generating responses that are more physiologically relevant so that cells can adhere, proliferate, migrate, and differentiate properly.[5]

The nervous system's complexity[4,6] necessitates careful selection of biomaterials, cell types, and growth factors to reproduce nervous system and neuro-related disorders *in vitro*. Both solid materials like poly(ε-caprolactone) (PCL),[4,6,7] poly(lactic-*co*-glycolic acid) (PLGA),[8–10] *etc.* and hydrogels created using the synthetic and/or natural precursor source have been applied. Among them, hydrogels stand out as promising materials for replicating neuronal development *in vitro* due to their high-water content, mechanical and structural properties and ability to mimic the biological milieu of the brain and the spinal cord.[11–15]

A key precursor material to produce hydrogels is the native extracellular matrix (ECM), a non-cellular 3D network of macromolecules in nervous tissue, which consists mainly of proteoglycans (PGs) and glycosaminoglycans (GAGs) and less fibrous proteins like collagens, elastin, fibronectin, laminins, and

[a] *Institute of Electronic Structure and Laser, Foundation for Research and Technology-Hellas (FORTH), Heraklion, 71003, Greece. E-mail: ranthi@iesl.forth.gr*
[b] *Department of Biology, University of Crete, Heraklion, 70013, Crete, Greece*
[c] *TECNALIA, Basque Research and Technology Alliance (BRTA), E20009, Donostia-San Sebastian, Spain*

several other glycoproteins.[16] GAG proteins like hyaluronic acid (HA), chondroitin sulfate, heparin, *etc.*, and proteoglycans are extremely hydrophilic, providing hydration to the brain tissue.[17,18] Decellularized ECMs derived from natural tissue provide mechanical and biochemical cues that support tissue structure and components that facilitate cell–cell and cell–matrix interactions which are essential for creating the ideal milieu for neural cell adhesion, survival, differentiation, and axon outgrowth throughout the process towards brain development and regeneration.[14,19]

3D hydrogels can be generated from decellularized ECMs of tissues such as the heart, lung, skin, and adipose tissue.[20] The decellularization process removes components that trigger an immune response from tissues using various physical, enzymatic, and chemical methods,[21,22] while preserving structural ECM proteins that provide significant signalling cues for stem cell migration, proliferation, survival, and differentiation.[23,24] Compared with substrates such as Matrigel or individual ECM components like collagen hydrogels, dECM hydrogels seem to enhance cell survival and differentiation, making them effective models for studying ECM functions in stem cell behavior and differentiation.[25,26]

Decellularized adipose tissue, first described by Flynn in 2010,[27] is an accessible source due to its abundance in the human or animal body and easy harvesting through procedures such as liposuction or abdominoplasty.[28] Rich in collagens, glycosaminoglycans, laminin, *etc.*,[22] and several bioactive molecules (growth factors and cytokines), it controls various biological processes such as inflammation, cell proliferation, and differentiation.[29] Importantly, the adipose-derived ECM maintains macrophage plasticity, promoting reparative phenotypes under healthy conditions while allowing proinflammatory responses during infection.[14,22]

Various studies have used ECM-derived or modified components of ECM hydrogels to create neural 3D *in vitro* models. For example, HA based 3D hydrogels have been preferred for promoting the differentiation of neural stem/progenitor cells into oligodendroglia and neuronal lineages while suppressing astroglia differentiation.[30] Umbilical cord dECM hydrogels have been explored for neural tissue repair,[23] and 3D ECM-derived matrices can create fully developed, interconnected dopaminergic neuron networks with improved differentiation and functionality.[31]

In our previous study, adECM was combined with reduced graphene oxide (rGO) to form dry, porous scaffolds aimed at enhancing neuronal differentiation *via* conductivity and stiffness modulation.[32] In contrast, the current work investigates the intrinsic bioactivity of solubilized, fully hydrated adECM hydrogels, free from any synthetic additives or exogenous materials. This allows us to explore how native topographical and biochemical properties of adipose-derived ECM alone influence neural stem cell fate within a more physiologically relevant 3D microenvironment.

This study focuses on the ability of neural stem cells (NSCs) to differentiate within 3D hydrogels derived from pure decellularized ECMs of porcine adipose tissue, a tissue-specific and underexplored source for neural applications. By encapsulating NSCs into hydrogels with two different ECM concentrations, the research aims to assess how native topographical and biochemical characteristics influence cellular behavior and differentiation pathways. While this study centers on fundamental aspects of NSC differentiation, the use of a fully biologically derived platform that closely mimics the natural microenvironment provides a promising basis for future development of physiologically relevant 3D neural *in vitro* models, with potential applications in neuroregeneration and neurodegeneration research.

## 2. Materials and methods

### 2.1. adECM pre-gel production

Adipose tissue was decellularised and delipidised as described in previous work.[14,22] These studies provide comprehensive characterization of the decellularized matrices, including residual DNA quantification and proteomic analysis of ECM components (*e.g.*, laminins, type IV collagen). Notably, the decellularized porcine-derived adipose matrix (pDAM) used in the present study meets the accepted decellularization criterion of $<50$ ng DNA/mg dry weight, with a residual DNA content of $24.8 \pm 2.05$ ng mg$^{-1}$, as reported by Cicuéndez *et al.* (2021).[22] Briefly, porcine adipose tissue was mechanically homogenised and centrifuged. Pellets were treated with isopropanol and Triton X-100, cleaned and lyophilised to obtain dry protein concentrates. The dried protein was milled to obtain adipose decellularised extracellular matrix (adECM) fine-grain powder. After the decellularisation process, hydrogels were obtained from acid-enzymatic digestion of the powder. adECM was digested for 48 hours at RT at a concentration of 15 mg ml$^{-1}$. Then, the acid solution was neutralised and equilibrated to physiologic pH and salt concentration.

### 2.2. Neuroectodermal stem cells (NE-4C cell line)

The NE-4C cell line was derived from murine neuroectodermal tissue, specifically the cerebral vesicles of 9-day-old mouse embryos lacking functional p53 genes.[33,34] The NE-4C cell line was purchased from ATTC (#CRL-2925) and maintained in the complete medium containing Eagle's minimum essential (EMEM, M4655, Sigma) supplemented with 10% (v/v) fetal bovine serum (FBS), 1% (v/v) penicillin–streptomycin mixture (P/S P4333, Sigma). Culture flasks had been coated with poly-L-lysine (PLL) (Sigma, P9155). Cell cultures were incubated in a controlled environment with 5% $CO_2$ at 95% humidity and at a constant temperature of 37 °C. Sub-confluent NE-4C cultures were regularly subcultured *via* trypsinization and the complete medium was refreshed every two days. Low passage NE-4C cells (3–8) were employed for all the experiments in this study.

### 2.3. Characterization of mechanical properties

The viscoelastic properties of adECM hydrogels were examined on a parallel-plate geometry (200-mm-diameter steel with a gap of 1 mm) using a Discovery Hybrid Rheometer HR 20 (TA instruments, New Castle, DE, USA). Dynamic frequency sweep

analysis was conducted in duplicate to measure the frequency-dependent storage ($G'$) and loss ($G''$) moduli of the hydrogels. All the measurements were made in constant deformation control mode over a frequency range of 0.01 to 10 Hz. All the measurements were carried out at 37 °C. The method was performed as previously described by Cicuéndez *et al.* (2024).[14]

### 2.4. Cell viability and metabolic activity

**2.4.1 Live/dead viability assay.** The viability of NSCs encapsulated in the 3D hydrogels was determined using the LIVE/DEAD™ viability/cytotoxicity Kit for mammalian cells (Thermofisher Scientific). The assay was performed on day 6 of culture to assess mid-term cell viability during the 10-day *in vitro* differentiation protocol. This time point was selected to determine whether the hydrogel environment could sustain cell viability beyond the acute response phase and into the differentiation period. Briefly, after 6 days of culture, the hydrogel containing the cells was removed from the culture medium and washed twice with Dulbecco's phosphate-buffered saline (D-PBS). In accordance with the manufacturer's recommendations, Calcein AM (excitation/emission: 494/517 nm) and Ethidium homodimer-1 (EthD-1) (excitation/emission: 528/617 nm) (stains dead cells) were diluted in Dulbecco's phosphate-buffered saline (D-PBS) to final concentrations of 2 μM and 4 μM, respectively, and applied to the cells. The staining reaction was incubated at 37 °C for 15 minutes. Dead cells were visualized using a 530 nm excitation wavelength, while live cells were observed under a 485 nm excitation wavelength using a Leica TCS SP8 inverted confocal microscope. To complement this assessment, cell metabolic activity at earlier time points (2 and 4 days) was evaluated using the PrestoBlue™ assay (see Section 2.4.2), providing additional insight into early-stage viability and confirming the absence of acute cytotoxic responses.

**2.4.2 PrestoBlue viability assay.** To investigate the metabolic activity, PrestoBlue™ Cell Viability Reagent assay (Invitrogen) was carried out in 24-well plates. The plate contained 2D culture ($10^4$ cells per well), 3D cell-encapsulated hydrogels ($25 \times 10^4$ cells per well), cell-free hydrogels with medium and only culture medium without cells as 2D and 3D background for correction of the samples, respectively. The variation in cell concentration is due to the differing dimensionality of the cultures. Treatment with PrestoBlue™ was conducted at 2, 4, and 6 days to evaluate the cytocompatibility. For the test, the cultured medium was removed and 600 μl of PrestoBlue solution (10% v/v in complete medium) was added to each well and the plate was incubated at 37 °C for 3 h. Later, 200 μl of the PrestoBlue solution from each well of the assay plates was transferred to a new 96-well plate, and the absorbance due to color change in the fluorescence of the reagent (resazurin to resorufin) was measured using an ELISA fluorescence multiwell plate reader (Biotek-Synergy HT) with the excitation/emission wavelengths set at 570 nm/600 nm. After the treatment, the hydrogels were washed with 1× PBS with calcium and magnesium to maintain cell integrity and then used for further incubation. The percentage of relative metabolic activity of cells (after subtracting the background) compared to the 2D controls was calculated using eqn (1):

$$\%\ \text{Relative metabolic activity} = \frac{\text{OD}_{(570-600\ \text{nm})\ \text{sample corrected}} - \text{OD}_{(570-600\ \text{nm})\ \text{background}}}{\text{OD}_{(570-600\ \text{nm})\ \text{average 2D control}} - \text{OD}_{(570-600\ \text{nm})\ \text{background}}} 100\% \quad (1)$$

### 2.5. *In vitro* differentiation of NE-4C cells

In the 2D culture experiments, NE-4C cells were seeded on poly-L-lysine-coated 24-well plates ($10^4$ cells per well). Following 4 days of proliferation, the cells underwent a 48-hour treatment with $10^{-6}$ M all-trans retinoic acid (RA) diluted in the complete medium. After RA induction, the medium was replaced with a serum-free neuronal differentiation medium composed of Dulbecco's modified Eagle's medium DMEM/F12 with HEPES nutrient medium (Sigma), supplemented with 1% v/v ITS; (I3146, Sigma) and 1% v/v B27 (17504044, Gibco) and 1% v/v P/S solution. The cells were kept in this medium for an additional 8 days, with the medium changed every two days.

In the 3D cultures, NE-4C cells were suspended in the complete medium and were mixed thoroughly with appropriate volumes of the pre-gel (15 mg $ml^{-1}$) to achieve final hydrogel concentrations of 7.5 and 10 mg $ml^{-1}$. Preliminary tests with 5 mg $mL^{-1}$ adECM hydrogels showed poor gelation and structural instability, which prevented consistent 3D culture of NSC neurospheres (see SI Fig. S1). Therefore, 7.5 and 10 mg $ml^{-1}$ were selected for further experiments. The encapsulated cell density in the hydrogel was $2.5 \times 10^6$ cells $ml^{-1}$. A volume of 100 μl of these encapsulated cells in hydrogels was then put in a 24-well plate ($25 \times 10^4$ cells per well), and incubated at 37 °C and 5% $CO_2$ for 30 minutes to complete the gelation process, forming hydrogel domes. The differentiation treatment for these 3D cultures was consistent with that of the 2D cultures. As control groups, we included both untreated and RA-treated cells to facilitate a comparative analysis relative to the experimental objectives.

### 2.6. Antibodies and reagents

The following antibodies and reagents were used: chicken anti-nestin 1/1000 (NB100-1604, Novus Biologicals), rabbit anti-ki67 1/1000 (ab15580, Abcam), chicken anti-GFAP 1/400 (AB5541, Sigma), mouse anti-tubulin β3 1/1000 (801 213, Biolegend), goat anti-mouse IgG-CF488 1/500 (20 010, Biotium), goat anti-rabbit IgG-CF555 1/500 (20 033, Biotium), goat anti-chicken IgG-Alexa Fluor-546 1/1000 (A-11040, ThermoScientific LSG), poly-L-lysine 15 μg $ml^{-1}$ (P9155, Sigma), all-trans retinoic acid (R2625, Sigma-Aldrich), and DAPI (Invitrogen™, SlowFade™ Diamond Antifade Mountant).

### 2.7. Immunocytochemistry assays

Undifferentiated NE-4C cells were fixed with 4% paraformaldehyde (PFA) solution in PBS for 15 min and treated with 0.1% v/v Triton-X in PBS for 5 min to facilitate permeabilization. After blocking for 30 min with 2% w/v BSA in PBS, primary and secondary antibodies were added subsequently and incubated

 

for 1 h at RT. After each incubation, 3 washes with PBS were performed. Finally, the samples were mounted on glass microscope slides with a mounting medium containing DAPI and examined under a confocal microscope.

Differentiated NE-4C cells were processed following a similar protocol. They were fixed with 1× Fixation Buffer (F1797, Sigma) in PBS for 15 min. This Fixation buffer, at a 10× concentration, contained 20% v/v formaldehyde, 2% v/v glutaraldehyde, 70.4 mM $Na_2HPO_4$, 14.7 mM $KH_2PO_4$, 1.37 M NaCl, and 26.8 mM KCl. After fixation, the staining procedure followed the same steps as described above for the undifferentiated cells.

### 2.8. Confocal and scanning electron microscopy (SEM)

Cell-encapsulated and cell-free hydrogel imaging was conducted using confocal microscopy and scanning electron microscopy (SEM), respectively. Neural stem cells were imaged using a Leica TCS SP8 inverted confocal microscope with either a 20× or 40× oil immersion objective lens. Confocal images were utilized to assess the quality of proliferation and differentiation processes, focusing on the expression of specific biomarkers. Each experiment was repeated at least three times, using more than three hydrogels from each adECM concentration. All images were processed using Fiji Image J software (version 2.14.0/1.53t).[35]

For SEM observation, cell-free hydrogels were fixed with a solution consisting of 2.5% w/v glutaraldehyde (GDA) and 2.5% w/v PFA diluted in 0.1 M sodium cacodylate buffer (SCB) for 30 min at 4 °C. Afterward, 3 washes with 0.1 M SCB at 4 °C were performed and specimens were dehydrated in a graded series of ethanol–water solutions, ultimately reaching 100% ethanol (30, 50, 60, 70, 80, 90, and 100%), with each step lasting 10–15 minutes. Instead of critical point drying, samples were dried with hexamethyldisilazane (HMDS), in an ethanol : HDMS ratio of 2 : 1 for 10 min, 1 : 1 for 5 min, and 100% HDMS for a quick wash and left to air dry overnight under a fume hood. Finally, a 15 nm layer of gold was sputter-coated onto the samples using a Baltec SCD 050 instrument (BAL-TEC AG, Balzers, Liechtenstein) and they were observed using SEM (JEOL JSM-6390 LV, Jeol USA Inc., Peabody, MA, USA) with an acceleration voltage of 15 kV.

To characterise the 3D hydrogel structure, SEM images at 20 000× magnification were processed using Fiji ImageJ software (version 2.14.0/1.53t).[35] Parameters such as average pore size, pore area distribution (% area), number of pores, and fiber diameter were quantified from three independent sets of images for each adECM concentration hydrogel. The analysis involved three steps: (1) image enhancement to ensure sufficient resolution and contrast for accurate analysis, (2) calculation of porosity percentage based on the areas of black (representing pores) and white (representing fibers) pixels using the 'Analyze Particles' function, following the method described by Anguiano M. *et al.*,[37] and (3) measurement and analysis of randomly selected fiber thickness for fiber diameter assessment.

### 2.9. Neuronal-lineage-specific gene expression

Prior to conducting quantitative PCR, total RNA was extracted and isolated from cell-encapsulated hydrogel constructs using TRIzol™ reagent (Invitrogen) following the manufacturer's instructions. Subsequently, RNA was converted into first-strand complementary DNA (cDNA) in a 20 mL reaction using a SuperScript® III First-Strand Synthesis System for RT-PCR (Invitrogen). Quantitative RT-PCR was carried out using the SYBR™ green master mix (SYBR™ Select Master Mix, Applied Biosystems™) with a 0.2 μM primer working solution. Genes of interest were amplified by the CFX96 touch real-time PCR detection system (Bio-Rad). To quantify the relative gene expression, we employed the ΔΔCt method. Actin beta (ACTB) was chosen as the reference gene for normalisation. To determine the fold change in the expression of each gene of interest following *in vitro* differentiation, ΔCt of the control group (untreated cells) was subtracted from ΔCt of each sample group to obtain ΔΔCt. Then, the $2^{-\Delta\Delta Ct}$ method was used to calculate the relative gene expression.[38] The primer list is outlined in Table 1.

### 2.10. Statistics

All experiments were carried out at least three times. The results are presented as means ± standard deviation (SD) of these independent experiments. For the different experiments, unpaired *t*-tests were performed for hydrogel characterization, two-way ANOVA for metabolic activity assay, and one-way ANOVA for qPCR analysis followed by the Tukey multiple comparison *post-hoc t*-test in order to draw comparisons between groups. All statistical analyses were performed in GraphPad Prism 8.0.2 software. Confidence intervals of 95% were adjusted with a Bonferroni correction and *p*-values $< 0.05$ were considered statistically different, marked by $*p < 0.05$, $**p < 0.01$, or $***p < 0.001$.

## 3. Results and discussion

### 3.1. Morphological and mechanical characterization of 3D adECM hydrogels

An ideal cell culture scaffold should allow space for cell seeding, growth, and proliferation while facilitating the diffusion of nutrients and the removal of metabolic waste products.[39,40] A comprehensive examination of the structural and topographical features of 3D matrices, particularly at the interface between the cell and hydrogel, provides valuable insights into the adaptations that occur as a result of cellular behavior.

Table 1 Genes and oligonucleotide primers used in qPCR analysis[a]

| Genes | Primer sequence (5′ to 3′) |
|---|---|
| ACTB | F: CGCCATGGATGACGATACG |
| | R: CGAAGCCGGCTTTGCACATG |
| NES | F: AAGTTCCCAGGCTTCTCTTG |
| | R: GTCTCAAGGGTATTAGGCAAGG |
| TUBB3 | F: CCTCACGCAGCAGATGTTCG |
| | R: GGATGTCACACACGGCTACC |
| SYP | F: TTGGCTTCGTGAAGGTGCTGCA |
| | R: ACTCTCCGTCTTGTTGGCACAC |
| GFAP | F: CTGATGTCTACCAGGCGGAGC |
| | R: CCAGGTTGTTCTCTGCCTCCAG |

[a] Sang H. Yoon, *et al.*[36]

The decellularized adECM used in this study has been previously validated in terms of DNA removal and ECM protein composition.[14,22] Given the focus of the current work on hydrogel microstructure and neural stem cell behavior, the characterization was not repeated here but is referenced to ensure reproducibility and protocol transparency.

SEM images revealed that adECM hydrogels exhibit important characteristics that mimic the tissue microenvironment. Specifically, at a concentration of 10 mg ml$^{-1}$, 3D adECM hydrogels form thicker and more densely grouped fibers compared to those at 7.5 mg ml$^{-1}$ 3D adECM hydrogels, yet both hydrogels create a wide range of pore size distribution network.

SEM figures (Fig. 1A–D) depict the differences in fiber diameter between the two concentrations of hydrogels. By measuring the length of random fibers it was confirmed that 10 mg ml$^{-1}$ hydrogels had thicker fibers than 7.5 mg ml$^{-1}$ hydrogels ($p < 0.001$) (Fig. 1E and F). These thicker fibers ranged in diameter from 65.2 to 177.7 nm, with a mean diameter of 110.3 nm, and frequently formed bundles of fibers (Fig. 1E and F and Table 2). In contrast, 7.5 mg ml$^{-1}$ hydrogels formed fibers with diameters ranging from 33.4 to 166.6 nm, with a mean of 86.6 nm (Fig. 1E and F and Table 2). As expected, a higher fiber density was observed in the 10 mg ml$^{-1}$ compared to the 7.5 mg ml$^{-1}$, due to the higher concentration used in the 10 mg ml$^{-1}$ pre-gel. This result is consistent with previous studies.[14] The SEM images of the two distinct concentrations of adECM hydrogels (7.5 mg ml$^{-1}$ and 10 mg ml$^{-1}$) reveal contrasting fiber architecture that could play a pivotal role in neural differentiation, particularly in the context of the neuron or astroglia formation, as suggested in previous literature.[41,42]

After conducting a comprehensive morphology characterization of 3D adECM hydrogels, quantified diagrams were used to highlight statistically significant differences ($p \leq 0.05$) in various structural parameters between the two hydrogel concentrations. Specifically, the analysis revealed that 7.5 mg ml$^{-1}$ 3D adECM hydrogels exhibited approximately 1401 ± 244 pores, with an average pore size of 6116 ± 1484 nm$^2$ covering an area of around 24 ± 4.8% (Fig. 1G–I and Table 2). In contrast, 10 mg ml$^{-1}$ 3D adECM hydrogels displayed a higher pore count, with approximately 1708 ± 230 pores observed in SEM images. The pores had an average size of approximately 3001 ± 1021 nm$^2$ and the covered area comprised around 16 ± 4.9% porosity (Fig. 1G–I and Table 2).

Although inter-fiber spacing was not directly measured, porosity serves as a robust structural parameter that reflects the overall void network. It captures features relevant to diffusion, cell infiltration, and encapsulation efficiency. Prior studies have established porosity as a key factor influencing neural cell migration and differentiation, often with greater predictive value than isolated fiber spacing.[43,44]

These results indicate that 7.5 mg ml$^{-1}$ 3D adECM hydrogels possess a structural configuration characterized by fewer and larger pores compared to their 10 mg ml$^{-1}$ counterparts, which create a denser network of more and smaller pores. In other words, the 7.5 mg ml$^{-1}$ 3D adECM hydrogels have a higher overall porosity area than the 10 mg ml$^{-1}$, as expected, because of the higher concentration of ECM components in the latter.

These findings align with previous observations in hydrogels composed of either natural materials like collagen[45,46] or synthetic materials like agarose,[47] where increasing the concentrations of

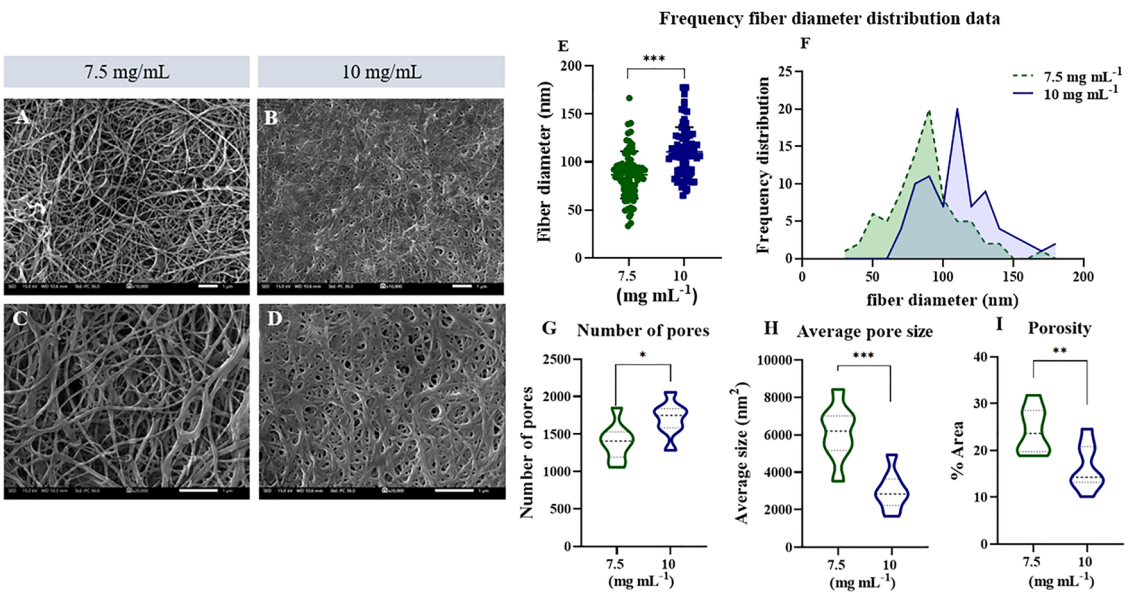


Fig. 1 Morphology and structure analysis of 3D adECM hydrogels based on SEM data. SEM images of cell-free (A) and (C) 7.5 mg mL$^{-1}$ and (B) and (D) 10 mg mL$^{-1}$ 3D adECM hydrogels at (A) and (B) 10.000× and (C) and (D) 20.000× magnification. Hydrogel cross-section (scale bars 1 μm). (E) and (F) Quantification of hydrogel's fiber diameter from SEM images. (E) The scatter graph represents the fibers' diameter distribution of the 7.5 and 10 mg mL$^{-1}$ adECM hydrogels (***$p < 0.01$). (F) Histogram depicts the frequency distribution of fibers' diameter after the cross-section of each hydrogel. (G)–(I) Quantification of adECM hydrogel morphological characteristics from SEM images. (G) Number of pores, (H) average of pore size, (I) porosity as % of pore area (student $t$-test, asterisks *, **, *** denote statistical difference $p < 0.05$, $p < 0.01$, and $p < 0.001$, respectively).

Table 2 Morphological characteristics of adECM hydrogels based on SEM data

| Porosity | | | | |
|---|---|---|---|---|
| | 7.5 mg ml$^{-1}$ | | 10 mg ml$^{-1}$ | |
| | Average | SD[a] | Average | SD[a] |
| Pore number | 1401 | 244 | 1708 | 230 |
| Area (%) | 24 | 4.8 | 16 | 4.9 |
| Average size (nm$^2$) | 6116 | 1486 | 3001 | 1021 |
| Fiber diameter | | | | |
| Fiber diameter (nm) | 86.6 | 24.5 | 110.3 | 25.8 |

[a] SD: standard deviation.

the precursor material results in a reduction of porosity and pore size.

The morphological characteristics were combined with and validated by the mechanical properties of the hydrogels. A higher polymer concentration has also been associated with increased mechanical properties. The denser extracellular matrix network shown in 10 mg ml$^{-1}$ formulation resulted in a higher storage and loss modulus than at 7.5 mg ml$^{-1}$ (Fig. 2). Nevertheless, the $G'$ to $G''$ ratio is similar, which confirmed that both formulations had a stronger solid than liquid behaviour due to the successful crosslinking process. The average storage modulus of 10 mg ml$^{-1}$ and 7.5 mg ml$^{-1}$ was 393 $\pm$ 30 Pa and 45 $\pm$ 5 respectively, meaning that adECM hydrogels with higher concentration required more energy to achieve the same deformation. The densely packed ECM fiber network enhanced intermolecular interactions, leading to a stiffer material.

### 3.2. Cell viability and metabolic activity

The Live/Dead assay results, as depicted in Fig. 3, revealed a remarkably high viability of NE-4C cells within the 3D adECM hydrogels. Evidently, the majority of encapsulated cells exhibited a vibrant green fluorescence after 6 days *in vitro*, indicating their continued survival. This outcome emphasizes the robust and supportive environment created by the hydrogels to sustain the viability of the enclosed NE-4C cells. This, in turn, validates the potential use of these hydrogels for various applications in cell-based research and tissue engineering.

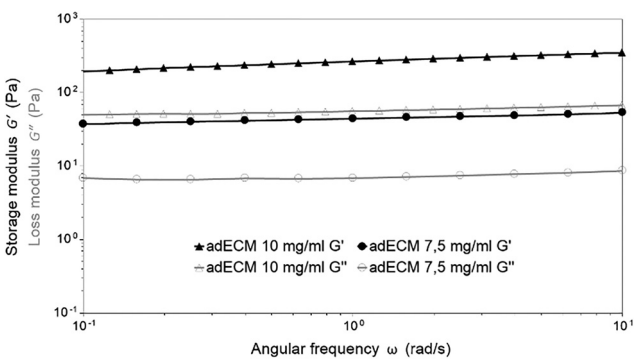


Fig. 2 Viscoelastic modulus of adECM hydrogels at 7.5 and mg ml$^{-1}$ concentration. Storage ($G'$, black) and loss ($G''$, grey) modulus are shown as a function of oscillatory angular frequency.

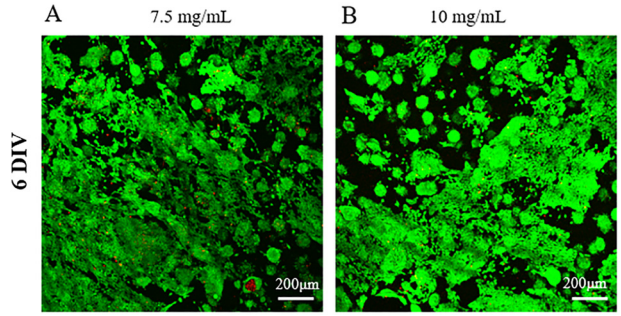


Fig. 3 Cell viability assay of encapsulated NE-4C cells in (A) 7.5 mg mL$^{-1}$ and (B) 10 mg mL$^{-1}$ 3D adECM hydrogel for 6 days *in vitro* (DIV). Live cells (Calcein, green) and dead cells (propidium iodide (PI), red) were stained. (scale bar 200 μm).

Simultaneously, the metabolic activity of encapsulated NE-4C cells in 3D adECM hydrogels was quantified by the PrestoBlue Cell Viability Reagent assay. Cell encapsulation was performed at concentrations of 7.5 and 10 mg ml$^{-1}$ 3D adECM hydrogels, and this assay was conducted over a 6-day *in vitro* (DIV) period. Notably, the PrestoBlue assay demonstrated stable metabolic activity throughout the 6-day duration (Fig. 4). At 6 days, both hydrogels exhibited significantly lower metabolic activity ($<0.05$) compared to 2D, though they maintained over 90% activity, which can be attributed to the spatial constraints within the hydrogels or limitations in nutrient diffusion. Nevertheless, both 2D and 3D culture systems retained metabolic activity beyond 4 and 6 DIV, indicating that the hydrogels are suitable for supporting the growth and differentiation of NSCs without inducing a cytotoxic effect.

### 3.3. Stemness and proliferation of encapsulated cells

To investigate cellular stemness and proliferation, NE-4C cells were encapsulated within 3D adECM hydrogels and cultured for 4 and 6 days. Subsequently, the cellular proliferation was assessed by examining the expression of Ki67, a nuclear protein

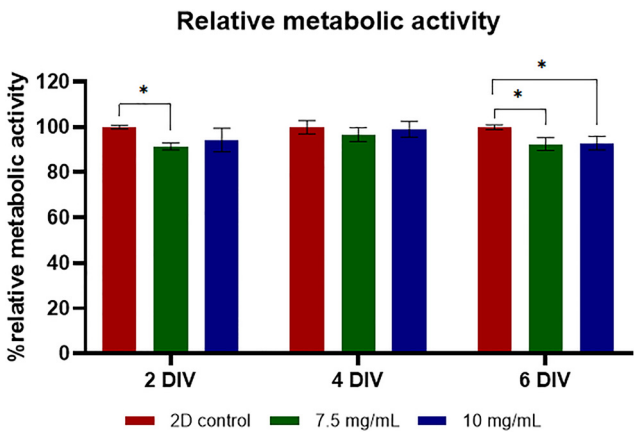


Fig. 4 Cellular metabolic activity was assessed using PrestoBlue™ cell viability reagent at 2, 4, and 6 days *in vitro* (DIV). Metabolic activity is expressed as a % relative metabolic activity after subtracting the 2D and 3D backgrounds (two-way ANOVA, * denote $p < 0.05$).

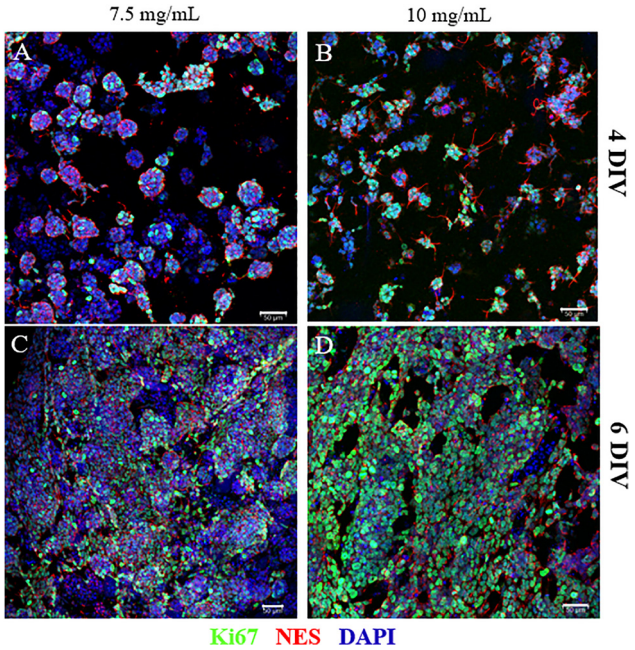


Fig. 5 Proliferation of NE-4C cells encapsulated in (A) 7.5 mg $mL^{-1}$ and (B) 10 mg $mL^{-1}$ 3D adECM hydrogels. Representative confocal images of NE-4C cells after 4 (A) and (B) and 6 (C) and (D) days *in vitro* (DIV). Cells were stained with DAPI (blue), Ki67 (green), and NES (red). In all images, the overlay is shown (scale bar 50 μm).

present during the G1, S, G2, and M phases of the cell cycle,[48] using confocal microscopy. Ki67 along with Nestin (NES) as a stemness indicator demonstrated robust cell growth, normal proliferation, and the preservation of stemness characteristics after 6 days. Notably, NE-4C cells typically require an external coating to facilitate survival, growth, and differentiation due to their challenging adhesion requirements. However, within 3D adECM hydrogels, they exhibited strong adhesion and sustained stemness and proliferation capability, indicating that hydrogels serve as a mimicking platform of the natural neural tissue microenvironment and eliminate the need for supplementary coating. The confocal images in Fig. 5 illustrate the stemness properties and sustained proliferation of encapsulated NE-4C cells, as evidenced by continued expression of $Ki67^{+}$ after 6 days *in vitro*. An indicative quantification of Ki67-positive cells is provided in SI Fig. S2, although interpretation is limited by neurosphere-like clustering and overlapping nuclei in the 3D environment. Importantly, these findings are consistent with live/dead staining and further supported by PrestoBlue metabolic assays, which provide quantitative evidence of sustained proliferation within the hydrogels.

### 3.4. Differentiation of encapsulated neural stem cells in 3D adECM hydrogels

To study the potential use of 3D adECM hydrogels as an *in vitro* system designed to recapitulate the brain microenvironment, NSCs were encapsulated in 3D adECM hydrogels and the differentiation ability, neurite outgrowth ability, and neural network formation were examined. In particular, to determine the effect on neuronal fate decisions, NE-4C cells were encapsulated in two different concentrations of 3D adECM hydrogels, proliferated for 4 days, and then treated with retinoic acid (RA) for 2 days to induce differentiation. After that, they were cultured for an additional 8-day period in a differentiation medium containing various neuronal supplements. This treatment results in a diverse population of undifferentiated cells (stroma cells), neurons, and astrocytes in the same culture. After the incubation period, the presence of neuronal and astrocyte populations was evaluated with confocal microscopy and RT-qPCR using the following chosen biomarkers. Nestin (NES), a neuroepithelial stem cell protein that forms cytoskeletal intermediate filaments, is temporally expressed in adult neural stem cells (NSCs) and immature neural progenitor cells, and its expression reduces as cells differentiate. Nestin has frequently been used as an NSC marker in both embryonic and adult brain tissue. Nestin is therefore widely accepted as a marker protein of undifferentiated CNS and PNS progenitors that give rise to neurons and glia.[49,50]

Tubulin beta 3 class III (TUBB3), another cytoskeletal protein expressed specifically in neurons, plays a key role in normal neurite elongation, axon guidance, and maintenance.[51] It has been demonstrated that the expression of TUBB3 is a useful tool for studying the early stages of neuronal differentiation in human and mouse embryonic development.[51,52] Synaptophysin (SYP), a glycoprotein found on the membrane of synaptic vesicles and widely expressed in the brain, contributes to synaptic development and plasticity (synaptogenesis). While it is primarily known for its role in neurotransmission and synapse formation, it also plays a role in neuronal regeneration, particularly in axonal growth and synaptic remodelling.[53] Regarding the astrocyte population, GFAP (glial fibrillary acidic protein) is an intermediate filament protein and a recognized astrocyte marker in the central nervous system (CNS), with its increased expression identified as an indicator of gliosis related to brain injury or disease.[54,55] The differentiation efficiency was evaluated compared to differentiated cells grown on PLL-coated 2D glass and undifferentiated cells. The latter served as the control group for RT-qPCR analysis for the relative expression of the mentioned neuronal lineage-specific genes.

The confocal imaging results revealed that 3D adECM hydrogels function as supportive scaffolds, promoting neural and astrocyte differentiation following RA induction. Cells that grew inwards and near neurospheres were flat and large resembling astrocytes with GFAP protein expression, while those that grew outwards from the spheres with small bodies and elongated fine processes were identified as neurons expressing TUBB3. In the hydrogels, a well-organized neural network was observed, characterized by dense axon bundles and close communication between numerous neurospheres (Fig. 6D–I). In contrast, the 2D culture system displayed thinner axons and a less robust neural network (Fig. 6A–C). This transition from a 2D to a 3D culture system influenced cellular behavior in terms of differentiation, resulting in a more complex neural network with greater and thicker axons extending outwards from the neurospheres in the 3D hydrogels.

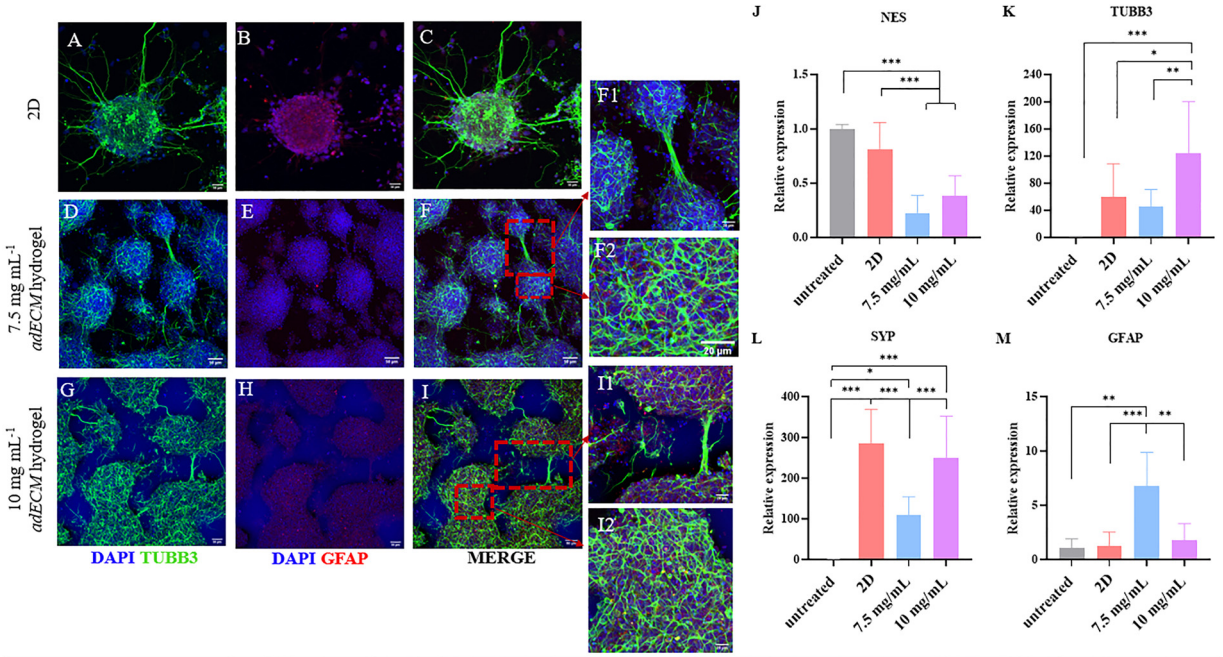


Fig. 6 Representative confocal images (A)–(I) and RT-qPCR quantification data (J)–(M) of the retinoic acid-induced differentiation of the encapsulated NE-4C cells in 3D adECM hydrogels after 10 days. Cells were stained with DAPI (blue), TUBB3 (green), and GFAP (red) (F1) and (F2) show zoomed-in regions of panel (F); panels (I1) and (I2) show zoomed-in regions of panel (I) (scale bar 50 μm). The graphs show the relative gene expression of (J): NES, (K): TUBB3, (L): SYP, and (M): GFAP. Relative gene expression is presented as normalized to Actin b (reference gene). Error bars represent the means ± SD. Statistical significance was determined with one-way ANOVA and Tukey *post-hoc* testing, asterisks *, **, and *** denote statistical differences $p < 0.05$, $p < 0.01$, and $p < 0.001$ respectively.

RT-qPCR analysis at 10 days of differentiation complemented these observations. The quantified results revealed a significant decrease ($p < 0001$) in NES expression (Fig. 6J) regardless of the adECM concentration in the hydrogels, indicating a favorable environment for NE-4C cell differentiation into mature neuronal lineages.

Moreover, the expression of TUBB3 was significantly higher in the 10 mg ml$^{-1}$ 3D adECM hydrogel group than in all other groups (Fig. 6K). In particular, TUBB3 expression was 120-fold, 2-fold, and 2,7-fold higher compared to untreated NE-4C, 2D, and 7.5 mg ml$^{-1}$ adECM hydrogel groups, respectively. SYP expression followed the same tendency as TUBB3 in the 10 mg ml$^{-1}$ 3D adECM hydrogel group with 300-fold more than the untreated group and 3-fold more than the 7.5 mg ml$^{-1}$ group (Fig. 6L). The 2D group appeared to express the same levels of SYP as the 10 mg ml$^{-1}$ 3D adECM hydrogel group.

Additionally, GFAP showed notable upregulation in the 7.5 mg ml$^{-1}$ 3D adECM hydrogel group, suggesting enhanced astrocyte differentiation (Fig. 6M). In particular, its expression was 7-fold higher whereas, in 2D and 10 mg ml$^{-1}$ 3D adECM hydrogel groups, GFAP expression was less than 2-fold compared to the untreated control group.

Together, our findings demonstrate that 3D adipose tissue-derived ECM (adECM) hydrogels serve as structurally suitable scaffolds supporting neuronal viability and differentiation showing that adipose ECM may offer unique differentiation cues. Notably, NE-4C cells encapsulated in 10 mg ml$^{-1}$ adECM hydrogels exhibited a pronounced increase towards neurons, as evidenced by the high expression levels of the TUBB3 and SYP genes. Conversely, the 7.5 mg ml$^{-1}$ adECM hydrogel indicated an apparent enhancement of astrocyte formation, characterized by elevated expression of the GFAP gene. These results support the assumption that biomechanical cues like topography could influence cell adhesion and differentiation fate decisions. Namely, the diameter and distribution of fibers inside hydrogels created a 3D environment that led to different levels of neuronal-lineage gene expression of NSCs cultured under differentiation conditions. Based on the analysis of adECM hydrogel topography, confocal and qPCR findings and comparing literature reports,[41,56,57] it has been shown that when fiber diameters are smaller than the dimensions of the cell, the cell attaches to multiple fibers and experiences forces pulling in different directions, leading to a well spread cell shape favoring astroglia formation (GFAP upregulation, $p < 0.01$). In contrast, when the fibers are thicker, the cell attaches to a single fiber, and the traction force acts in only one direction leading to neuron development (TUBB3 and SYP upregulation, $p < 0.05$). These differences in fiber thickness and matrix stiffness, based on our viscoelastic results, likely modulate integrin-mediated mechanotransduction pathways, including FAK, RhoA/ROCK, and YAP/TAZ signaling, which regulate cytoskeletal tension and ultimately influence lineage commitment. Stiffer matrices with thicker fibers enhance focal adhesion formation and cytoskeletal contractility, promoting neuronal differentiation, whereas softer matrices with thinner fibers reduce cytoskeletal tension, favoring astrocytic fate. Although our study characterized

hydrogel structures using SEM and rheology, more comprehensive quantitative analyses of microstructural features such as pore size distribution and fiber orientation will be valuable in future work to better correlate matrix properties with neural stem cell differentiation outcomes. Unlike our previous study employing reduced graphene oxide (rGO)-reinforced adECM foamed scaffolds,[32] which were rigid and dry, the current hydrogels are fully hydrated and composed solely of native adECM without conductive additives or crosslinkers. This allows a cleaner investigation of the intrinsic biochemical and mechanical cues of adipose-derived ECMs in a soft, 3D microenvironment, free from external stimuli like rGO-induced conductivity or stiffness.

Thus, this model provides a more reductionist and mechanistically defined approach to studying ECM–NSC interactions in neural differentiation.

However, several limitations of our model must be acknowledged. The NE-4C cell line used in this study was derived from p53-deficient mouse embryos.[33] Since p53 loss has been shown to promote neuronal differentiation,[58,59] this characteristic may have influenced the differentiation patterns we observed. The role of p53 in neural development is still not fully understood and appears to be complex and context-dependent. Therefore, these results should be interpreted with caution, and further studies using models with intact p53 function are needed to fully understand the underlying mechanisms. Additionally, while Nestin and Ki67 were used to assess stem/progenitor status and proliferation, the inclusion of other key stemness markers such as SOX2 would provide a more comprehensive analysis. Future work will incorporate SOX2 immunostaining and/or gene expression profiling to strengthen the characterization of NSC identity within the 3D hydrogel environment. In summary, these findings not only validate the ability of pure adipose-derived ECM hydrogels to support NSC viability and differentiation but also reveal how modest variations in ECM concentration and microarchitecture can direct lineage outcomes. Unlike previous studies that rely on brain-derived ECM or synthetic matrices, this work pioneers the use of the adipose tissue-derived ECM as a fully biological and accessible scaffold for neural applications. This innovative integration of a native ECM-based hydrogel with a 3D neurosphere model offers a mechanistically informed and translationally relevant platform advancing our ability to model neurodevelopment and neurodegeneration *in vitro* and laying the foundation for scalable, animal-free alternative for neural tissue engineering and preclinical research. Our results highlight the potential of adECM hydrogels as biomimetic *in vitro* tools; however, *in vivo* studies are essential to evaluate their integration, immunocompatibility, and functional relevance.

While the current study focused on early-to-mid differentiation stages, future work will involve extended culture periods and longitudinal analyses to assess how the hydrogel supports sustained cell viability, progressive differentiation, and functional maturation over time.

## 4. Conclusions

This study demonstrates the effectiveness of 3D hydrogels derived from adipose tissue ECMs in promoting the differentiation of neural stem cells (NSCs). By encapsulating NSCs in these hydrogels, which closely mimic the *in vivo* 3D brain environment, the research revealed how varying ECM concentrations influence cellular behavior, especially in differentiation processes. While differences in fiber structure and pore formation had minimal impact on cellular proliferation, they did influence differentiation into neuronal lineages, as shown by distinct gene expression. Additionally, variations in ECM concentration altered the mechanical stiffness of the hydrogels, though both formulations exhibited similar viscoelastic behavior. These biomechanical and microstructural cues likely modulate integrin-mediated mechanotransduction pathways, which in turn regulate lineage commitment and neural cell fate decisions. These findings emphasize the potential of 3D adECM hydrogels as more accurate and effective *in vitro* models for neural tissue engineering, introducing an innovative approach that combines native ECM-derived materials with a neurosphere-based 3D culture system. This integrated strategy offers a novel perspective on how scaffold architecture can be engineered to guide neural cell fate. With their ability to closely replicate key features of the brain microenvironment, these models represent a significant advancement over traditional 2D systems and synthetic scaffolds. Additionally, by offering a more physiologically realistic platform that better predicts cellular behaviors, these models address the major gap in preclinical studies and are in line with the global demand for alternatives to animal testing. Although our findings establish a strong foundation for using adECM hydrogels as *in vitro* platforms, *in vivo* models remain essential to fully capture the complex vascular, immunological, and multicellular interactions of the native neural niche. Future studies incorporating *in vivo* validation, detailed microstructural quantification, and assessments of functional maturation will further strengthen the translational relevance of this platform. These advancements could lead to the development of more predictive 3D brain models for studying neural development and neurodegenerative disorders, and identifying new therapeutic strategies.

## Author contributions

Kyriaki Stampouli: writing – original draft, methodology, data curation, and investigation. Lina Papadimitriou: writing – review & editing, methodology, and conceptualization. Andrea García-Lizarribar: writing – review & editing, methodology, and investigation. Iratxe Madarieta: writing – review & editing and methodology. Beatriz Olalde: writing – review & editing, conceptualization, resources, and funding acquisition. Anthi Ranella: writing – review & editing, supervision, conceptualization, visualization, and funding acquisition.

## Conflicts of interest

There are no conflicts to declare.

## Data availability

Data for this article are available at: **https://cloud.iesl.forth.gr/index.php/s/jzior2YScxwaxyt**.

Supplementary information is available. See DOI: **https://doi.org/10.1039/d5ma00310e**.

## Acknowledgements

This work was supported by the European Union's Horizon 2020 Research and Innovation Programme (H2020-FETOPEN-20182020, NeuroStimSpinal Project, Grant Agreement No. 829060), and also by NFFA EUROPE Pilot (EU 2020 framework programme) under grant agreement no. 101007417 from 1/03/2021 to 28/02/2026. The authors would also like to acknowledge Mrs Aleka Manoussaki (IESL, FORTH) for her valuable contribution to the SEM analysis and Mr Eleftherios Spanos for his contribution to the graphical abstract design.

## References

1 L. J. Marshall, J. Bailey, M. Cassotta, K. Herrmann and F. Pistollato, *Altern. Lab Anim.*, 2023, **51**, 102–135.
2 R. C. Hubrecht and E. Carter, *Animals*, 2019, **9**, 754.
3 World Health Organisation [WHO], 2024, **https://www.who.int/news-room/fact-sheets/detail/the-top-10-causes-of-death**.
4 G. Tarricone, I. Carmagnola and V. Chiono, *J. Funct. Biomater.*, 2022, **13**, 146.
5 J. Kapr, L. Petersilie, T. Distler, I. Lauria, F. Bendt, C. M. Sauter, A. R. Boccaccini, C. R. Rose and E. Fritsche, *Adv. Healthcare Mater.*, 2021, **10**(16), DOI: **10.1002/adhm.202100131**.
6 P. Nikolakopoulou, R. Rauti, D. Voulgaris, I. Shlomy, B. M. Maoz and A. Herland, *Brain*, 2020, **143**, 3181–3213.
7 Z. Javkhlan, S.-H. Hsu, R.-S. Chen and M.-H. Chen, *J. Dent. Sci.*, 2024, **19**, 1096–1104.
8 E. Saylam, Y. Akkaya, E. Ilhan, S. Cesur, E. Guler, A. Sahin, M. E. Cam, N. Ekren, F. N. Oktar, O. Gunduz, D. Ficai and A. Ficai, *Appl. Sci.*, 2021, **11**, 10727.
9 Y. Polo, J. Luzuriaga, J. Iturri, I. Irastorza, J. L. Toca-Herrera, G. Ibarretxe, F. Unda, J.-R. Sarasua, J. R. Pineda and A. Larrañaga, *Nanomedicine*, 2021, **31**, 102314.
10 I. Manero-Roig, Y. Polo, B. Pardo-Rodríguez, J. Luzuriaga, R. Basanta-Torres, D. Martín-Aragón, I. Romayor, S. Martín-Colomo, J. Márquez, L. Gomez-Santos, F. Lanore, Y. Humeau, G. Ibarretxe, C. Eguizabal, A. Larrañaga and J. R. Pineda, *Methods in Cell Biology*, Elsevier, 2024, vol. 188, pp. 237–254.
11 S. R. Caliari and J. A. Burdick, *Nat. Methods*, 2016, **13**, 405–414.
12 L. Papadimitriou, P. Manganas, A. Ranella and E. Stratakis, *Mater. Today Bio*, 2020, **6**, 100043.
13 C. Kasper, D. Egger and A. Lavrentieva, eds, *Basic Concepts on 3D Cell Culture*, Springer International Publishing, Cham, 2021.
14 M. Cicuéndez, A. García-Lizarribar, L. Casarrubios, M. J. Feito, F. J. Fernández-San-Argimiro, N. García-Urkia, O. Murua, I. Madarieta, B. Olalde, R. Diez-Orejas and M. T. Portolés, *Biomater. Adv.*, 2024, **159**, 213794.
15 Y. Polo, J. Luzuriaga, S. Gonzalez De Langarica, B. Pardo-Rodríguez, D. E. Martínez-Tong, C. Tapeinos, I. Manero-Roig, E. Marin, J. Muñoz-Ugartemendia, G. Ciofani, G. Ibarretxe, F. Unda, J.-R. Sarasua, J. R. Pineda and A. Larrañaga, *Nanoscale*, 2023, **15**, 4488–4505.
16 D. Lam, H. A. Enright, J. Cadena, S. K. G. Peters, A. P. Sales, J. J. Osburn, D. A. Soscia, K. S. Kulp, E. K. Wheeler and N. O. Fischer, *Sci. Rep.*, 2019, **9**, 4159.
17 K. Pogoda, R. Bucki, F. J. Byfield, K. Cruz, T. Lee, C. Marcinkiewicz and P. A. Janmey, *Biomacromolecules*, 2017, **18**, 3040–3051.
18 M. Cieśluk, K. Pogoda, E. Piktel, U. Wnorowska, P. Deptuła and R. Bucki, *Brain Sci.*, 2022, **12**, 927.
19 N. J. Fiore, J. D. Tamer-Mahoney, A. Beheshti, T. J. F. Nieland and D. L. Kaplan, *Biomaterials*, 2022, **290**, 121858.
20 V. E. Getova, J. A. Van Dongen, L. A. Brouwer and M. C. Harmsen, *Artif. Cells, Nanomed., Biotechnol.*, 2019, **47**, 1693–1701.
21 M. Song, Y. Liu and L. Hui, *Mol. Med. Rep.*, 2018, **17**(1), 138–146.
22 M. Cicuéndez, L. Casarrubios, M. J. Feito, I. Madarieta, N. Garcia-Urkia, O. Murua, B. Olalde, N. Briz, R. Diez-Orejas and M. T. Portolés, *Int. J. Mol. Sci.*, 2021, **22**, 3847.
23 Z. Kočí, K. Výborný, J. Dubišová, I. Vacková, A. Jäger, O. Lunov, K. Jiráková and Š. Kubinová, *Tissue Eng., Part C*, 2017, **23**, 333–345.
24 O. A. Mohiuddin, B. Campbell, J. N. Poche, C. Thomas-Porch, D. A. Hayes, B. A. Bunnell and J. M. Gimble, in *Cell Biology and Translational Medicine, Volume 6*, ed. K. Turksen, Springer International Publishing, Cham, 2019, vol. 1212, pp. 57–70.
25 G. S. Hussey, J. L. Dziki and S. F. Badylak, *Nat. Rev. Mater.*, 2018, **3**, 159–173.
26 G. G. Giobbe, C. Crowley, C. Luni, S. Campinoti, M. Khedr, K. Kretzschmar, M. M. De Santis, E. Zambaiti, F. Michielin, L. Meran, Q. Hu, G. Van Son, L. Urbani, A. Manfredi, M. Giomo, S. Eaton, D. Cacchiarelli, V. S. W. Li, H. Clevers, P. Bonfanti, N. Elvassore and P. De Coppi, *Nat. Commun.*, 2019, **10**, 5658.
27 L. E. Flynn, *Biomaterials*, 2010, **31**, 4715–4724.
28 T. Ibsirlioglu, A. E. Elçin and Y. M. Elçin, *Methods*, 2020, **171**, 97–107.
29 A. E. Anderson, I. Wu, A. J. Parrillo, M. T. Wolf, D. R. Maestas, I. Graham, A. J. Tam, R. M. Payne, J. Aston, C. M. Cooney, P. Byrne, D. S. Cooney and J. H. Elisseeff, *npj Regener. Med.*, 2022, **7**, 6.
30 S. K. Seidlits, J. Liang, R. D. Bierman, A. Sohrabi, J. Karam, S. M. Holley, C. Cepeda and C. M. Walthers, *J. Biomed. Mater. Res.*, 2019, **107**, 704–718.
31 L. Rueda-Gensini, J. A. Serna, D. Rubio, J. C. Orozco, N. I. Bolaños, J. C. Cruz and C. Muñoz-Camargo, *Biofabrication*, 2023, **15**, 045001.

32 N. Barroca, D. M. Da Silva, S. C. Pinto, J. P. M. Sousa, K. Verstappen, A. Klymov, F.-J. Fernández-San-Argimiro, I. Madarieta, O. Murua, B. Olalde, L. Papadimitriou, K. Karali, K. Mylonaki, E. Stratakis, A. Ranella and P. A. A. P. Marques, *Biomater. Adv.*, 2023, **148**, 213351.
33 K. Schlett and E. Madarasz, *J. Neurosci. Res.*, 1997, **47**, 405–415.
34 B. V. Varga, N. Hádinger, E. Gócza, V. Dulberg, K. Demeter, E. Madarász and B. Herberth, *BMC Dev. Biol.*, 2008, **8**, 89.
35 C. A. Schneider, W. S. Rasband and K. W. Eliceiri, *Nat. Methods*, 2012, **9**, 671–675.
36 S.-H. Yoon, M.-R. Bae, H. La, H. Song, K. Hong and J.-T. Do, *Int. J. Mol. Sci.*, 2021, **22**, 8322.
37 M. Anguiano, C. Castilla, M. Maška, C. Ederra, R. Peláez, X. Morales, G. Muñoz-Arrieta, M. Mujika, M. Kozubek, A. Muñoz-Barrutia, A. Rouzaut, S. Arana, J. M. Garcia-Aznar and C. Ortiz-de-Solorzano, *PLoS One*, 2017, **12**, e0171417.
38 K. J. Livak and T. D. Schmittgen, *Methods*, 2001, **25**, 402–408.
39 J. Lee, M. J. Cuddihy and N. A. Kotov, *Tissue Eng., Part B*, 2008, **14**, 61–86.
40 Z. Abpeikar, P. B. Milan, L. Moradi, M. Anjomshoa and S. Asadpour, *Mech. Adv. Mater. Struct.*, 2022, **29**, 4911–4922.
41 G. T. Christopherson, H. Song and H.-Q. Mao, *Biomaterials*, 2009, **30**, 556–564.
42 M. G. Tupone, M. d'Angelo, V. Castelli, M. Catanesi, E. Benedetti and A. Cimini, *Front. Bioeng. Biotechnol.*, 2021, **9**, 639765.
43 H. Zhao, T. Xiong, Y. Chu, W. Hao, T. Zhao, X. Sun, Y. Zhuang, B. Chen, Y. Zhao, J. Wang, Y. Chen and J. Dai, *Small*, 2024, **20**(32), DOI: **10.1002/smll.202311456**.
44 Z. Li, Y. Qi, L. Sun, Z. Li, S. Chen, Y. Zhang, Y. Ma, J. Han, Z. Wang, Y. Zhang, H. Geng, B. Huang, J. Wang, G. Li, X. Li, S. Wu and S. Ni, *Theranostics*, 2023, **13**, 4762–4780.
45 T. Fischer, A. Hayn and C. T. Mierke, *Sci. Rep.*, 2019, **9**, 8352.
46 E. Monferrer, S. Martín-Vañó, A. Carretero, A. García-Lizarribar, R. Burgos-Panadero, S. Navarro, J. Samitier and R. Noguera, *Sci. Rep.*, 2020, **10**, 6370.
47 I. Jayawardena, P. Turunen, B. C. Garms, A. Rowan, S. Corrie and L. Grøndahl, *Mater. Adv.*, 2023, **4**, 669–682.
48 T. Scholzen and J. Gerdes, *J. Cell. Phys.*, 2000, **182**, 311–322.
49 J. Dahlstrand, M. Lardelli and U. Lendahl, *Dev. Brain Res.*, 1995, **84**, 109–129.
50 S. Suzuki, J. Namiki, S. Shibata, Y. Mastuzaki and H. Okano, *J. Histochem. Cytochem.*, 2010, **58**, 721–730.
51 J. Guo, M. Qiang and R. F. Ludueña, *Brain Res.*, 2011, **1420**, 8–18.
52 J. Zhang and J. Jiao, *BioMed Res. Int.*, 2015, **2015**, 1–14.
53 L. Zhao, J.-W. Liu, B.-H. Kan, H.-Y. Shi, L.-P. Yang and X.-Y. Liu, *World J. Stem Cells*, 2020, **12**, 1576–1590.
54 E. M. Hol and M. Pekny, *Curr. Opin. Cell Biol.*, 2015, **32**, 121–130.
55 A. Messing and M. Brenner, *ASN Neuro*, 2020, **12**, 175909142094968.
56 H. B. Wang, M. E. Mullins, J. M. Cregg, C. W. McCarthy and R. J. Gilbert, *Acta Biomater.*, 2010, **6**, 2970–2978.
57 E. A. Silantyeva, W. Nasir, J. Carpenter, O. Manahan, M. L. Becker and R. K. Willits, *Acta Biomater.*, 2018, **75**, 129–139.
58 A. Ferreira and K. S. Kosik, *J. Cell Sci.*, 1996, **109**, 1509–1516.
59 Y. Xiong, Y. Zhang, S. Xiong and A. E. Williams-Villalobo, *Biology*, 2020, **9**, 285.